Journal of Molecular Liquids 384 (2023) 122285

Contents lists available at ScienceDirect

Journal of Molecular Liquids

journal homepage: www.elsevier.com/locate/molliq

Microplastics as an adsorption and transport medium for per- and polyfluoroalkyl substances in aquatic systems: Polystyrene and undecafluorohexanoic acid interactions

Katalin Bere [a], Xiong Xiong [a], Szilárd Sáringer [a], Grant Douglas [b,c], Istvan Szilagyi [a,*]

[a] MTA-SZTE Lendület Biocolloids Research Group, Department of Physical Chemistry and Materials Science, Interdisciplinary Excellence Center, University of Szeged, H-6720 Szeged, Hungary
[b] Centre for Environment and Life Sciences, CSIRO Environment, WA-6913 Wembley, Australia
[c] School of Molecular and Life Sciences, Curtin University, WA-6102 Bentley, Australia

A B S T R A C T

The assessment of possible interactions between microplastic particles (MPP) and other emerging contaminants such as per- and polyfluoroalkyl substances (PFAS) is of great importance due to their potentially conjunctive harmful effects on the environment. Here, the colloidal behaviour of a polystyrene MPP in the presence of undecafluorohexanoic acid (UFHA), an alternative to the widely used C8 PFAS, was studied in aqueous dispersions. Adsorption of UFHA on MPP was confirmed, where it induced charge neutralization with overcharging at higher UFHA concentrations. Rates of MPP aggregation were rapid with neutral particles, while slow at low and high UFHA doses, where considerable, alternate surface charge persisted and hence, fine particle dispersion was maintained. The addition of multivalent ions influenced the surface charge and aggregation features of MPP, in both their native form and in the presence of UFHA. Concurrent adsorption of electrolytes and UFHA was observed and strongly affected the rate of MPP aggregation under some experimental conditions. This study provides new insights into the possible interactions of PFAS with MPP, which may fundamentally influence the migration of these contaminants in aqueous environments. Aggregated particles will more likely accumulate in the sediments or at the air–water interface, while individual, highly stable MPP-PFAS composites have the potential to migrate together in the water column.

1. Introduction

Plastic pollution, and particular that of microplastics is now recognized as a major contemporary global problem [1–3]. Currently, million tons of plastic waste are added to the environment every year [4] with the extent of plastic pollution continuing to increase [5–8]. Following its introduction to the environment, fragmentation of plastic occurs due to one or more of mechanical destruction or abrasion, UV degradation, or chemical oxidation resulting in the formation of micro- and nano-sized particles [9–12]. At present, the size distribution-based nomenclature can be considered to be somewhat contradictory. From the colloid and materials chemistry point of view, plastic particles with diameter below 100 nm are considered as nanoplastics, while above this threshold value they named as microplastic particles (MPP). The upper limit is also questionable, but 5000 μm is the most used upper size [13]. However, MPP of between 100 and 1000 nm in diameter are of particular interest, since in this size range they possess classical colloidal properties [14]. The colloidal properties not only influence their migration in the environment, but their ability to enter into living organisms, with MPP detected in biomass as diverse as the human placenta [15,16], fish [17] and plants [2,18,19] with a potential to induce substantial health risks [20–22].

Interaction of MPP with other materials especially in aqueous environment is a crucial issue in terms of assessing the potential migration and ecotoxicity [23,24]. It has been previously reported that dissolved organic matter [25], drug molecules [26], radionuclides [27], and bacteria [28] are able to adsorb on MPP leading to modification of the surface properties and of the colloidal behaviour of MPP [29]. In particular, the interaction between emerging contaminants [30,31] and MPP is crucial to understand, since their assembly may give rise to as yet unquantified risks to the environment.

Per- and polyfluoroalkyl substances (PFAS) are now recognised as widespread and persistent environmental pollutants [32,33]. PFAS consist of a long fluorinated carbon chain, with a functional group at the end of the molecule, most commonly carboxyl or sulfonate [34] that collectively endow surfactant-like properties [35]. PFAS are widely used in industrial processes, e.g., in production of firefighting foams, paints, pesticides and in everyday consumer products such as food packaging

* Corresponding author.
E-mail address: szistvan@chem.u-szeged.hu (I. Szilagyi).

https://doi.org/10.1016/j.molliq.2023.122285
Received 24 February 2023; Received in revised form 4 June 2023; Accepted 5 June 2023
Available online 7 June 2023

materials, non-stick cookware and cosmetics [36,37]. Due to the strong C-F bonds, the PFAS are chemically very stable compounds, and while the functional groups may be subject to transformation in the environment (e.g., from fluorotelomers), the fluorinated chain is considered persistent in nature [38].

The effects of PFAS exposure on humans, animals, or plants has been assessed by numerous ecotoxicological and epidemiological-based studies. Many common PFAS compounds (e.g., perfluorooctanoic acid - PFOA, perfluorooctane sulfonic acid - PFOS) are implicated in an increased risks of the development of some cancers, thyroid diseases, immuno-, reproductive-, and developmental-disorders and hepatotoxicity [36,37,39].

Whilst the presence of MPP and PFAS may be considered ubiquitous, in particular in urban aquatic systems, their extent of interaction to form a novel composite is as yet largely unknown as is the potential impact on the wider environment [24]. For example, migration of MPP in natural waters primarily depends on their size and surface charge properties. Such particles collide and thereafter may remain independent or form aggregates depending on the predominating interparticle forces amongst other factors including particle velocity and solution shear. Upon aggregation, they may settle or alternatively may form a detergent-like micellar scum leading to accumulation in the sediment or at the air–water interface, respectively [40]. Although these colloidal features have been previously investigated with MPP [5,14,41–43], the effect of PFAS on surface charge and aggregation processes of MPP has yet to be systematically studied.

To address this knowledge gap in the interaction of these two widespread environmental pollutants, polystyrene MPP were synthesized, and their colloidal stability was investigated in the presence of undecafluorohexanoic acid (UFHA also known as perfluorohexanoic acid - PFHxA) via measurement of surface charge and aggregation rate using light scattering techniques, with the experimental results were compared to model predictions. UFHA was used in this study as it has been applied as a C6 alternative to the C8 PFAS used frequently in the fluoropolymer industry. Importantly, UFHA has been already detected in the environment [44]. Its interaction, however, with MPP has not been studied. In addition, the effect of dissolved electrolytes of different valences on the dispersion properties of MPP and MPP-PFAS was also assessed.

2. Materials and methods

2.1. Chemicals

Laboratory grade HCl (37 %), KCl (~99.5 %), $MgCl_2{\cdot}6H_2O$ (~99.0 %) and absolute ethanol (≥99.8 %) were bought from VWR, while $LaCl_3$ (~99.9 %) and undecafluorohexanoic acid (UFHA) (≥97.0 %) from Sigma-Aldrich. Styrene (99 %) and 2,2′-azobis(2-methylpropionamidine) dihydrochloride (AIBA) initiator (≥98.0 %) were purchased from Acros Organics and Hellmanex III cleaning agent from Hellma. The solutions were prepared with ultrapure water, using a Puranity TU 3 UV/UF + system and filtered with PVDF-based 0.1 μm syringe filters (Millex-VV). The pH was maintained at (4.0 ± 0.2) in all stock dispersions and solutions used for sample preparation by adding appropriate amount of HCl or KOH (both from Sigma-Aldrich) solutions. The pH was checked with a combined glass electrode connected to a benchtop pH meter (WTW inoLab).

2.2. MPP synthesis

Positively charged polystyrene particles were prepared based on previously reported methods [45,46] using an additive-free emulsion polymerization reaction with AIBA as the initiator. In the first step, 375 mL water was stirred for 15 min, and the temperature was increased progressively to 80 °C. Thereafter, 10 g of styrene monomers were added to the water and the solution was stirred for 15 min. Subsequently, 0.2 g of AIBA (0.04 w%) was dissolved in 115 mL deionized water and put into the reaction mixture. The temperature was kept at 80 °C for 24 h under a nitrogen atmosphere. After the mixture was cooled to room temperature, the remaining styrene and AIBA were removed by repeated washing, centrifugation, and re-dispersing steps. The precipitated product was washed with HCl, water, and ethanol (three times 1 M HCl, once with ethanol, and three times with water) and dialyzed against water for a day using cellulose ester membrane with a molecular mass cut-off of 50 kg/mol (Spectrum). The final solid concentration was 10 g/L in the stock dispersion, which was stored in fridge thereafter. The MPP are positively charged due to the presence of AIBA initiator, which is a widely applied cationic initiator in surfactant-free polymerization reactions [45].

2.3. Infrared spectroscopy

The Fourier-transform infrared spectroscopy (FTIR) spectrum of MPP was recorded on a Summit FTIR spectrometer (Nicolet Instrument Corporation) with attenuated total reflection detection mode using ZnSe-based accessories. The spectra were collected in the range of 4000–400 cm^{-1} with 4 cm^{-1} resolution and 16 scans.

2.4. Transmission electron microscopy

The morphology of the MPP was examined with transmission electron microscopy (TEM). The particles were dried on a copper-coated carbon mesh TEM grid and were imaged using a TECNAI G2 20 X-TWIN instrument (FEI) with 200 kV accelerating voltage.

2.5. Electrophoretic light scattering

Zeta potentials were measured by a Litesizer 500 device (Anton Paar) outfitted with a 658 nm wavelength laser source. The applied voltage was 200 V. The primarily determined electrophoretic mobilities were converted to zeta potential data using the Smoluchowski equation [47] shown in the Supplementary Data (SD) in Eq S1. The MPP stock dispersion was homogenized by sonication prior to the sample preparation, during which the particles were added to calculated amount of salt solutions and water leading to a total volume of 2.0 mL. The final particle concentration was always 25 mg/L. The samples were equilibrated at room temperature for 2 h and 700 μL of the dispersion was transferred to omega cuvettes (Anton Paar) with eight consecutive measurements, whose average value was reported.

2.6. Dynamic light scattering

Dynamic light scattering (DLS) measurements were performed with either an ALV/CGS-3 compact goniometer system (ALV GmbH) or a Litesizer 500 device. The diffusion coefficient was determined from the decay rate of the autocorrelation function (Eq S2) obtained from the second order cumulant fit and was converted to hydrodynamic radius with the Stokes-Einstein equation [48,49] shown in Eq S3. During time-resolved experiments to determine apparent aggregation rate constants (Eq S4), the duration of one run was 20 s and 80 repetitions were carried out in borosilicate glass cuvettes (Kimble Chase). The total volume of each sample was 2.0 mL, in which the particle concentration was 5 or 10 mg/L depending on the speed of aggregation. The UFHA dose was varied in a concentration range of 1–10000 μM. In a typical experiment, 0.2 mL of MPP stock dispersion was added to 1.8 mL aqueous solution of UFHA and/or salt (KCl, $MgCl_2$ or $LaCl_3$). The DLS measurements commenced immediately after vortex homogenization of the mixture. The colloidal stability was expressed in terms of stability ratio, which was determined from the increase in the hydrodynamic radii, i.e., from the apparent rate values, in aggregating particle dispersions (Eq S5). Note that stability ratio is one in case of rapid or diffusion-controlled aggregation, while larger for slow aggregation. Hence, the inverse of the stability ratio is

equal to the fraction of particle collision resulting in formation of particle dimers. It is a commonly used parameter to describe stability of colloidal dispersions [48,50–53]. The temperature was kept at (25.0 ± 0.2) ℃ in all (both electrophoretic and dynamic) light scattering measurements, in which the UFHA concentration was always at least 5-time below its solubility limit reported elsewhere [54].

3. Results and discussion

3.1. MPP characterisation

Transmission electron microscopy images recorded in dried state confirm the formation of the MPP as indicated by the spherical particles (Fig. 1a and Fig. S1). Analysing the particle size distribution on the TEM images resulted in an average radius of (83 ± 22) nm.

Based on DLS measurements, an average hydrodynamic radius of (110 ± 3) nm and a polydispersity index of (0.11 ± 0.05) were determined (Fig. 1b). These values and the exponential decay of the autocorrelation functions together with their excellent reproducibility (Fig. S2) indicated a narrow MPP size distribution in aqueous dispersion. The larger DLS radius compared to the one determined with TEM is due to the higher contribution of the bigger particles to the scattered intensity [55] and to the fact that DLS measures the geometrical radius together with the thickness of the hydrodynamically stagnant layer on the particles [49] in contrast to TEM size, which is determined in dried stage.

FTIR spectroscopy was used to identify typical peaks corresponding to C–H and C═C bonds and methylene groups characteristic of unreacted styrene monomer. The spectra are shown in Fig. S3 while the peak assignment to the stretching and bending vibrations is listed in Table S1 in the SD. The data confirmed the formation of the polystyrene MPP.

3.2. Behaviour of MPP in different ionic environments

The behaviour of MPP in aqueous environments strongly depends on their colloidal stability, i.e., dispersed, stable particles have a propensity to spread rapidly, while aggregates may either settle or form surface scums. Dissolved electrolytes of various valences influence these processes since they modify the MPP surface charge upon adsorption as well as contribute to the ionic strength in larger extent. Ion specific affinities alter the balance of interparticle forces, as reported earlier based on results of direct force measurements [56–58]. The rate of aggregation and surface charge features of the present polystyrene MPP were investigated by determining both stability ratios and zeta potentials in various salt solutions (Fig. 2). A pH value of (4.0 ± 0.2) was chosen for the experiments because the MPP possess significant positive charge due to ionization of its functional groups, the multivalent metal ions applied do not hydrolyze, i.e., maintain their valence [59,60], as well as the UFHA is fully deprotonated [54] under this experimental condition.

In general, the stability ratio of MPP progressively decreased by increasing the salt concentration until the critical coagulation concentration (CCC), irrespective of the cation valence (Fig. 2a for K^+, Fig. 2b for Mg^{2+} and Fig. 2c for La^{3+}). The CCC was calculated using Eq S6 and Eq S7 (see SD). This CCC separates the slow and fast aggregation regimes, i.e., the threshold salt concentration value, beyond which the dispersion can be considered as unstable indicated by stability ratios close to unity (Fig. 2a–c). A slight increase in the stability ratios at the highest salt concentrations can be attributed to the increased solute viscosity and hence, a retardation of the aggregation rate.

Zeta potentials decreased with increasing the salt concentrations in all systems. For K^+ (Fig. 2a) and Mg^{2+} (Fig. 2b), the potentials were close to zero at high salinity, while for La^{3+} (Fig. 2c), they remained near +15 mV even at the highest salt concentrations. These observations imply the presence of two phenomena. First, the ions screen the surface charge, thus progressively decreasing the zeta potential with increasing ionic strength. This is a well-established phenomenon for the charging behaviour of colloids in electrolyte solutions provided the constant surface charge approximation applies [52,56–58,61,62]. Second, specific adsorption of La^{3+} on the like-charged surface of MPP likely occurred and provided a positive charge for the particles even at high salt levels due to competitive effects between charge screening and direct La^{3+} interaction with the surface. Such an adsorption of weakly hydrated multivalent co-ions (ions with the same sign of charge as the surface) has also been observed for negatively charged titania [51] and plastic [63] particles. However, this is the first known occurrence with MPP of positive surface charge.

Variations in the stability ratios and in the zeta potentials can be explained by classic DLVO theory [52,64]. Accordingly, the overall interparticle forces originate from the superposition of the electrostatic repulsion by the overlapping electrical double layers and the attractive van der Waals forces. The former is sensitive to the salt concentration, while the latter is not, so persists irrespective of solute composition. Therefore, increasing the salt concentration leads to diminishing double layer forces, which may vanish up to and beyond the CCC. Thus, at low salt concentrations, the electrostatic repulsion is strong and stabilizes the dispersions, while at high salinity, van der Waals attractions predominate, and the MPP undergo diffusion-controlled aggregation. The above interpretation was further confirmed by comparing the experimentally measured CCC data with theoretical predictions (Fig. 3).

The CCC values were determined for KCl at 72.4 mM, for $MgCl_2$ at 19.8 mM and for $LaCl_3$ at 8.0 mM. Such a decrease in the CCC data by increasing the valence of coions is consistent with the inverse Schulze-Hardy rule [65] established for the destabilization power of

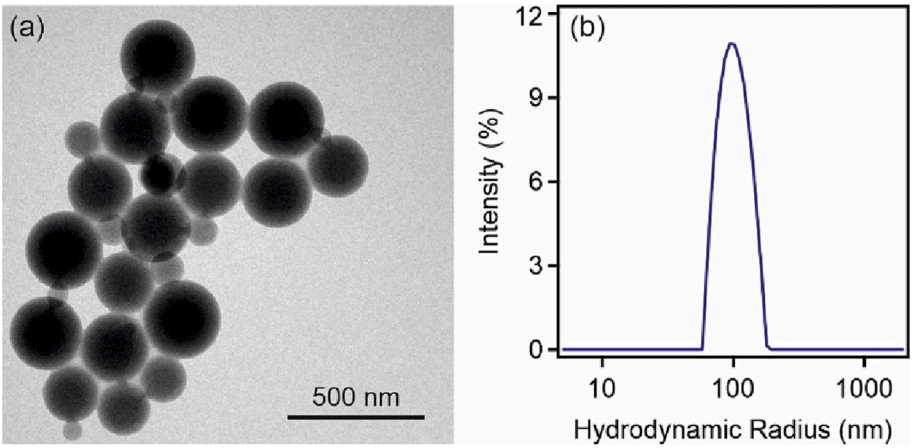

Fig. 1. A representative TEM image (a) and intensity weighted DLS size distribution (b) of MPP.

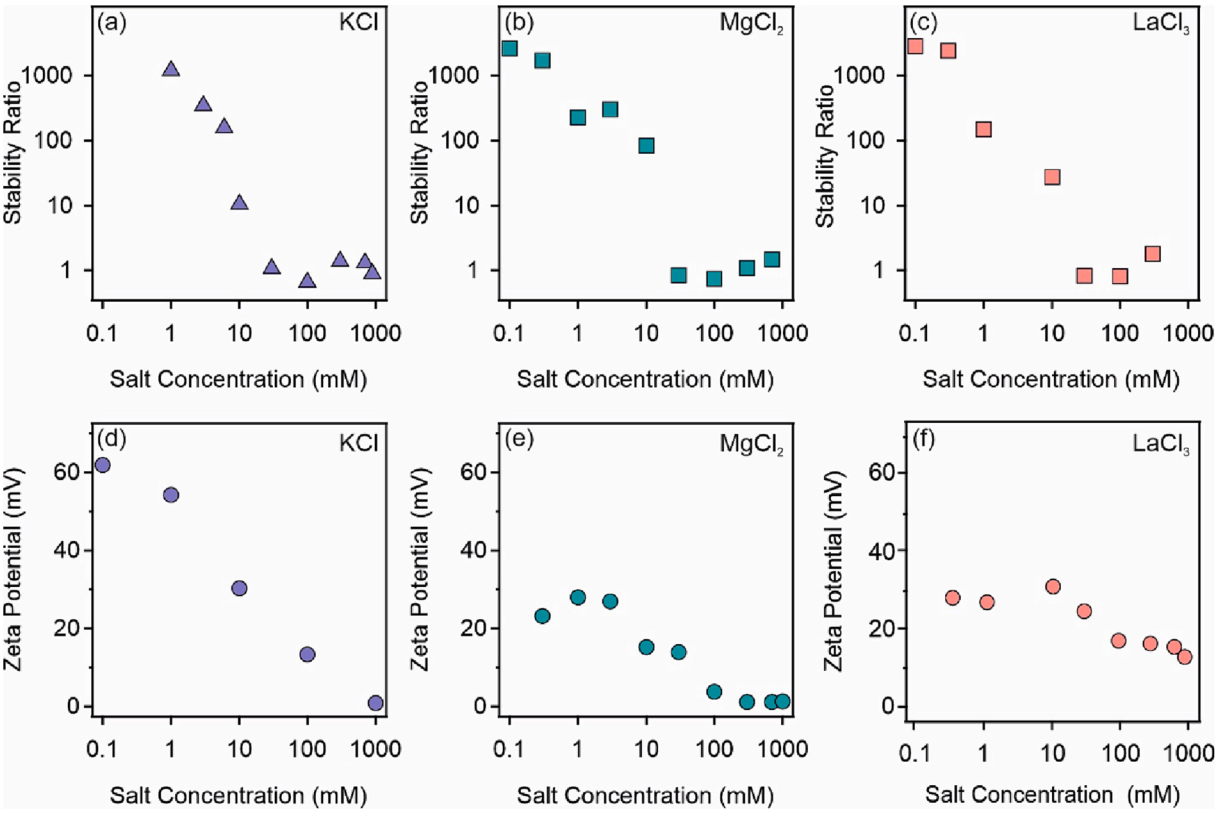

Fig. 2. Top row: stability ratio of MPP determined in KCl (a), $MgCl_2$ (b) and $LaCl_3$ (c) solutions. Salt concentration equals to metal ion concentration in the samples. Bottom row: zeta potential values of MPP as a function of the KCl (d), $MgCl_2$ (e) and $LaCl_3$ (f) concentrations.

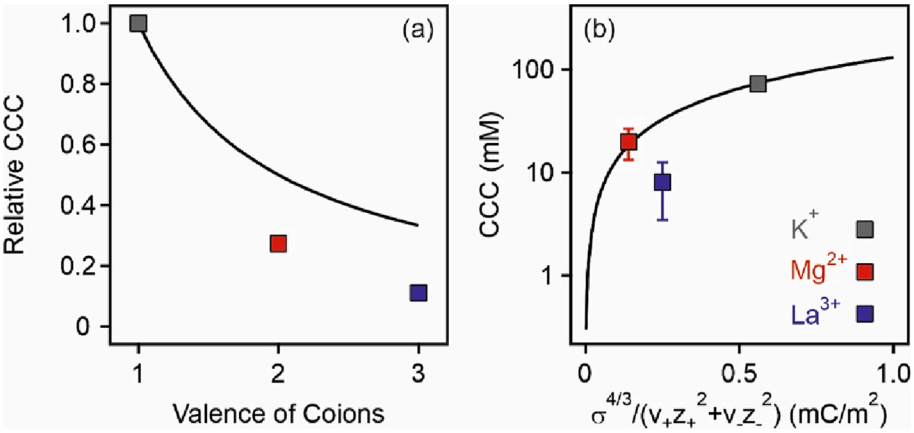

Fig. 3. (a) Relative CCC of MPP (normalized to the CCC obtained in the KCl system) as a function of the valence of co-ions. The solid line indicates the *CCC* $1/z$ prediction according to the inverse Schulze-Hardy rule. (b) Dependence of the CCC on the charge density was normalized to the salt stoichiometry and valence. The symbols are experimental points, while the solid line was calculated with Eq S9.

multivalent co-ions (Fig. 3a). However, the decrease in the experimental CCC compared to the theoretical values is substantial. This variance may reflect additional (non-DLVO) attractive forces, not accounted for by the inverse Schulze-Hardy model, are present.

The Debye-Hückel model [52] was used to obtain charge densities at the slip plane from the ionic strength dependence of the zeta potentials (Eq S8) and these data were used to calculate the CCC values according to the DLVO theory, refer to Eq S9 and Eq S10 [66]. The agreement between experimental and calculated data is excellent in the systems containing K^+ and Mg^{2+} (Fig. 3b) indicating that the particle aggregation is consistent with electrostatic theory. For La^{3+}, however, a lower CCC was determined experimentally, i.e., DLVO theory predicts the onset of rapid particle aggregation at higher La^{3+} concentrations. This suggests the presence of additional attractive forces. The zeta potential data indicate La^{3+} adsorption on the MPP leading to positive surface charge at elevated salt concentrations. Such adsorption could induce formation of hydrophilic regions on the hydrophobic surface of MPP which may attract proximal particles. Similar interactions were observed between polystyrene surfaces across electrolyte solutions at short separation distances [57,58].

3.3. Interaction of MPP and UFHA

In aqueous media, UFHA is deprotonated due to the presence of the

strongly electron-withdrawing fluorocarbon tail. Hence, it is expected to strongly adsorb on the positively charged MPP surface. To investigate the nature of the MPP-UFHA interaction, zeta potentials were measured at different UFHA spanning four magnitudes of concentration (Fig. 4).

In all systems, UFHA adsorption on the MPP was indicated by a gradual reduction in surface charge and change of sign of the surface charge with progressively increasing the UFHA concentration. At low UFHA levels, the positive charge of the MPP dominated, but at approximately 1 mM, adsorption gave rise to charge neutralization at the isoelectric point (IEP) followed by subsequent overcharging of the particles with increasing concentrations. These charging features, with charge reversal in similar surfactant concentration regimes, have also been observed upon adsorption of non-fluorinated, amphiphilic surface-active agents on plastic [67,68] and inorganic [53,69,70] particles.

In terms of colloidal stability for the MPP in the presence of UFHA, unstable dispersions with stability ratios close to unity were experienced near the IEP, while slow particle aggregation processes were observed far from these conditions. Such a behaviour resulted in V- (for K^+ and Mg^{2+}) and U-shaped (for La^{3+}) curves, while the plateaus in the stability ratio data at low and high UFHA doses suggest moderate aggregation of native MPP due to surface adsorption of UFHA. Substantial differences were apparent in the width of the unstable regimes, which occupies a much wider concentration region for La^{3+} (Fig. 4f) than for K^+ (Fig. 4d) or Mg^{2+} (Fig. 4e).

These variations in the stability ratio data are consistent with the DLVO theory, with particle aggregation principally governed by the superposition of DLVO-type repulsive electrical double layer and attractive van der Waals forces. Similar results on various particle–surfactant (non-PFAS) systems have been documented elsewhere [53,67–70]. Accordingly, a striking difference can be observed between the colloidal behaviour of MPP in the absence (Fig. 2) and presence (Fig. 4) of UFHA.

Furthermore, noticeable deviations were observed in the IEP, which were 0.80 mM in KCl (Fig. 4a), 1.00 mM in $MgCl_2$ (Fig. 4b) and 1.85 mM in $LaCl_3$ (Fig. 4c) solutions. This trend is also apparent for zeta potentials measured at 10 mM UFHA concentrations, at which the overcharging effect is the most pronounced (Fig. 5).

The concurrent increase in the IEP with the valence suggests that adsorption of multivalent ions took place on the like-charged MPP, as discussed earlier. Such adsorption increases the surface charge and thus, a higher concentration of oppositely charged UFHA is needed to reach

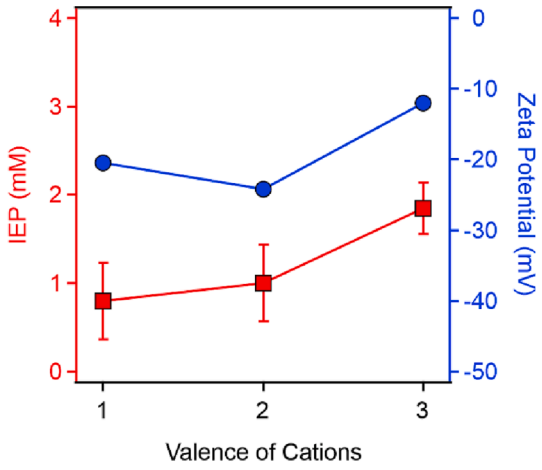

Fig. 5. IEP data (left axis, squares) of the MPP in the presence of UFHA and zeta potentials (right axis, circles) determined at 10 mM UFHA concentrations as a function of the cation valence in KCl, $MgCl_2$ and $LaCl_3$ solutions. The solid lines are just to guide the eyes.

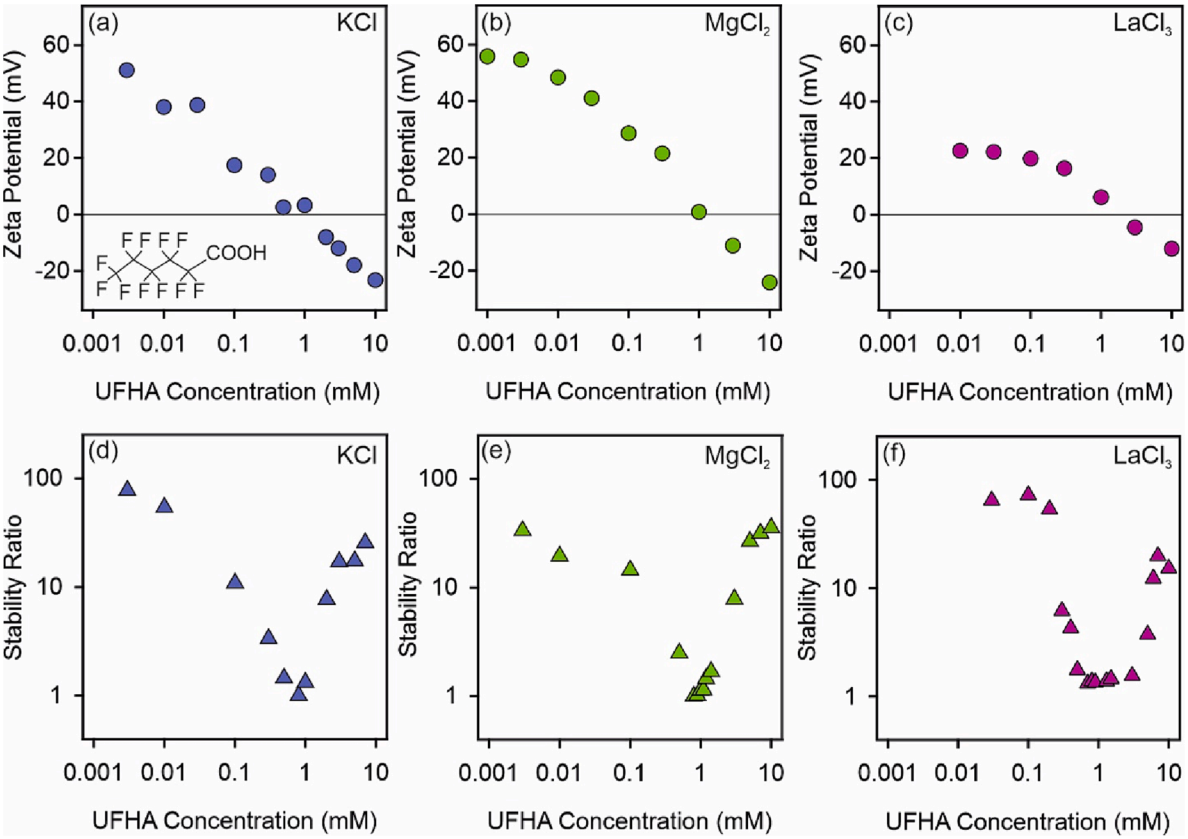

Fig. 4. Zeta potentials (top row) and stability ratios (bottom row) as a function of the UFHA concentration in 1 mM KCl (a, d), $MgCl_2$ (b, e) and $LaCl_3$ (c, f) solutions. The structure of UFHA is shown in the inset of (a). The continuous lines serve to guide the eyes.

the IEP. This phenomenon is the most pronounced in the case of La^{3+}, whose considerable adsorption has been already demonstrated (Fig. 2f). The zeta potential data at 10 mM UFHA concentrations is significantly lower in the presence of La^{3+} than in K^{+} and Mg^{2+} solutions under the given experimental conditions. This also suggests significant adsorption of La^{3+}, which results in net less negative MPP-UFHA composites upon overcharging.

4. Conclusions

The colloidal behaviour of MPP in the presence of UFHA, a widely used newer generation C6 PFAS, and/or electrolytes of different valences was studied. Both the surface charge and aggregation of MPP were sensitive to the concentration and valence of the dissolved salt constituents. Reduced colloidal stabilities were observed with increasing the salinity due to the concurrent effect of salt screening and specific ion adsorption. In contrast to K^{+} and Mg^{2+}, in La^{3+} solutions, multivalent ions were able to adsorb on the like-charged MPP and thus, significant surface charge was maintained even at elevated concentrations. The MPP stability regimes were quantitatively determined and were consistent with DLVO theory, however, additional attractive forces induced by La^{3+} accumulation on the surface were also identified. Adsorption of UFHA was confirmed and led to charge neutralization at the IEP and overcharging at high concentrations. This charging behaviour was sensitive to the valence of K^{+}, Mg^{2+} and La^{3+} cations. Larger IEP values were observed due to the joint adsorption of La^{3+} and UFHA on the MPP surface. At low and high UFHA doses, the MPP systems were stable, while rapid particle aggregation took place near the IEPs. This study has identified a significant affinity of UFHA with the MPP surface indicating a potential for concurrent migration of these contaminants in aqueous environments. However, such transport of PFAS by MPP can be limited by the colloidal stability of the samples, which strongly depends on the conditions such as MPP-to-PFAS ratio as well as presence of electrolytes of different concentrations and valences.

CRediT authorship contribution statement

Katalin Bere: Data curation, Investigation, Validation, Methodology, Writing – original draft. **Xiong Xiong:** Methodology, Investigation, Writing – original draft. **Szilárd Sáringer:** Data curation, Investigation. **Grant Douglas:** Conceptualization, Writing – review & editing. **Istvan Szilagyi:** Supervision, Conceptualization, Writing – review & editing, Resources, Project administration.

Declaration of Competing Interest

The authors declare that they have no known competing financial interests or personal relationships that could have appeared to influence the work reported in this paper.

Data availability

Data will be made available on request.

Acknowledgements

Financial support from the National, Research, Development and Innovation Office via projects TKP2021-NVA-19 and SNN142258 is gratefully acknowledged. The assistance in FTIR measurements by Adél Szerlauth is highly appreciated. The support from the University of Szeged Open Access Fund (No. 6326) is gratefully acknowledged.

Appendix A. Supplementary material

Supplementary data to this article can be found online at https://doi.org/10.1016/j.molliq.2023.122285.

References

[1] D.M. Mitrano, M. Wagner, A sustainable future for plastics considering material safety and preserved value, Nat. Rev. Mater. 7 (2022) 71–73.
[2] M. Sendra, E. Sparaventi, B. Novoa, A. Figueras, An overview of the internalization and effects of microplastics and nanoplastics as pollutants of emerging concern in bivalves, Sci. Total Environ. 753 (2021), 142024.
[3] Y. Pico, A. Alfarhan, D. Barcelo, Nano- and microplastic analysis: Focus on their occurrence in freshwater ecosystems and remediation technologies, Trends Anal. Chem. 113 (2019) 409–425.
[4] J. Ma, J.H. Zhao, Z.L. Zhu, L.Q. Li, F. Yu, Effect of microplastic size on the adsorption behavior and mechanism of triclosan on polyvinyl chloride, Environ. Pollut. 254 (2019), 113104.
[5] O.S. Alimi, J.F. Budarz, L.M. Hernandez, N. Tufenkji, Microplastics and nanoplastics in aquatic environments: Aggregation, deposition, and enhanced contaminant transport, Environ. Sci. Technol. 52 (2018) 1704–1724.
[6] X.T. Zhang, Y.X. Chen, X.Y. Li, Y.L. Zhang, W. Gao, J. Jiang, A.Y. Mo, D.F. He, Size/shape-dependent migration of microplastics in agricultural soil under simulative and natural rainfall, Sci. Total Environ. 815 (2022), 152507.
[7] T. Gardon, M. El Rakwe, I. Paul-Pont, J. Le Luyer, L. Thomas, E. Prado, K. Boukerma, A.L. Cassone, V. Quillien, C. Soyez, L. Costes, M. Crusot, C. Dreanno, G. Le Moullac, A. Huvet, Microplastics contamination in pearl-farming lagoons of French Polynesia, J. Hazard. Mater. 419 (2021), 126396.
[8] J. Brahney, M. Hallerud, E. Heim, M. Hahnenberger, S. Sukumaran, Plastic rain in protected areas of the United States, Science 368 (2020) 1257–1260.
[9] J. Talvitie, A. Mikola, A. Koistinen, O. Setala, Solutions to microplastic pollution - Removal of microplastics from wastewater effluent with advanced wastewater treatment technologies, Water Res. 123 (2017) 401–407.
[10] P. Pfohl, M. Wagner, L. Meyer, P. Domercq, A. Praetorius, T. Huffer, T. Hofmann, W. Wohlleben, Environmental degradation of microplastics: How to measure fragmentation rates to secondary micro- and nanoplastic fragments and dissociation into dissolved organics, Environ. Sci. Technol. 56 (2022) 11323–11334.
[11] S. Ducoli, S. Federici, R. Nicsanu, A. Zendrini, C. Marchesi, L. Paolini, A. Radeghieri, P. Bergese, L.E. Depero, A different protein corona cloaks "true-to-life" nanoplastics with respect to synthetic polystyrene nanobeads, Environ. Sci.-Nano 9 (2022) 1414–1426.
[12] D.M. Mitrano, P. Wick, B. Nowack, Placing nanoplastics in the context of global plastic pollution, Nat. Nanotechnol. 16 (2021) 491–500.
[13] A.K. Kniggendorf, C. Wetzel, B. Roth, Microplastics detection in streaming tap water with Raman spectroscopy, Sensors 19 (2019) 1839.
[14] A. Al Harraq, B. Bharti, Microplastics through the lens of colloid science, ACS Environ, Au 2 (2022) 3–10.
[15] A. Ragusa, A. Svelato, C. Santacroce, P. Catalano, V. Notarstefano, O. Carnevali, F. Papa, M.C.A. Rongioletti, F. Baiocco, S. Draghi, E. D'Amore, D. Rinaldo, M. Matta, E. Giorgini, Plasticenta: First evidence of microplastics in human placenta, Environ. Int. 146 (2021), 106274.
[16] L. Zhu, J.Y. Zhu, R. Zuo, Q.J. Xu, Y.H. Qian, L.H. An, Identification of microplastics in human placenta using laser direct infrared spectroscopy, Sci. Total Environ. 856 (2023), 159060.
[17] J. Bhagat, L.Q. Zang, N. Nishimura, Y. Shimada, Zebrafish: An emerging model to study microplastic and nanoplastic toxicity, Sci. Total Environ. 728 (2020), 138707.
[18] J.C. Prata, J.P. da Costa, I. Lopes, A.L. Andrady, A.C. Duarte, T. Rocha-Santos, A One Health perspective of the impacts of microplastics on animal, human and environmental health, Sci. Total Environ. 777 (2021), 146094.
[19] L. Yang, Y.L. Zhang, S.C. Kang, Z.Q. Wang, C.X. Wu, Microplastics in soil: A review on methods, occurrence, sources, and potential risk, Sci. Total Environ. 780 (2021) 20.
[20] Y.X. Jin, J.Z. Xia, Z.H. Pan, J.J. Yang, W.C. Wang, Z.W. Fu, Polystyrene microplastics induce microbiota dysbiosis and inflammation in the gut of adult zebrafish, Environ. Pollut. 235 (2018) 322–329.
[21] S. Sharma, S. Chatterjee, Microplastic pollution, a threat to marine ecosystem and human health: a short review, Environ. Sci. Pollut. Res. 24 (2017) 21530–21547.
[22] L.G.A. Barboza, A.D. Vethaak, B. Lavorante, A.K. Lundebye, L. Guilhermino, Marine microplastic debris: An emerging issue for food security, food safety and human health, Mar. Pollut. Bull. 133 (2018) 336–348.
[23] P.A. Athulya, N. Chandrasekaran, Interactions of natural colloids with microplastics in aquatic environment and its impact on FTIR characterization of polyethylene and polystyrene microplastics, J. Mol. Liq. 369 (2023), 120950.
[24] M.M. Rahman, M.B. Sultan, M. Alam, Microplastics and adsorbed micropollutants as emerging contaminants in landfill: A mini review, Curr. Opin. Environ. Sci. Health 31 (2023), 100420.
[25] Y. Sun, J. Ji, J. Tao, Y. Yang, D. Wu, L. Han, S. Li, J. Wang, Current advances in interactions between microplastics and dissolved organic matters in aquatic and terrestrial ecosystems, Trends Anal. Chem. 158 (2023), 116882.
[26] R. Nugnes, C. Russo, M. Lavorgna, E. Orlo, M. Kundi, M. Isidori, Polystyrene microplastic particles in combination with pesticides and antiviral drugs: Toxicity and genotoxicity in Ceriodaphnia dubia, Environ. Pollut. 313 (2022), 120088.
[27] I. Ioannidis, I. Anastopoulos, I. Pashalidis, Neptunium interaction with microplastics in aqueous solutions, J. Mol. Liq. 356 (2022) 4.
[28] A. Kruglova, B. Munoz-Palazon, A. Gonzalez-Martinez, A. Mikola, R. Vahala, J. Talvitie, The dangerous transporters: A study of microplastic-associated bacteria passing through municipal wastewater treatment, Environ. Pollut. 314 (2022), 120316.

[29] X.X. Wang, Y.T. Dan, Y.Z. Diao, F.H. Liu, H. Wang, W.J. Sang, Y.L. Zhang, Transport characteristics of polystyrene microplastics in saturated porous media with biochar/Fe_3O_4-biochar under various chemical conditions, Sci. Total Environ. 847 (2022) 9.
[30] S.D. Richardson, S.Y. Kimura, Water analysis: Emerging contaminants and current issues, Anal. Chem. 92 (2020) 473–505.
[31] I. Anastopoulos, I. Pashalidis, B. Kayan, D. Kalderis, Microplastics as carriers of hydrophilic pollutants in an aqueous environment, J. Mol. Liq. 350 (2022), 118182.
[32] C.F. Kwiatkowski, D.Q. Andrews, L.S. Birnbaum, T.A. Bruton, J.C. DeWitt, D.R. U. Knappe, M.V. Maffini, M.F. Miller, K.E. Pelch, A. Reade, A. Soehl, X. Trier, M. Venier, C.C. Wagner, Z.Y. Wang, A. Blum, Scientific basis for managing PFAS as a chemical class, Environ. Sci. Technol. Lett. 7 (2020) 532–543.
[33] A. Podder, A. Sadmani, D. Reinhart, N.B. Chang, R. Goel, Per and poly-fluoroalkyl substances (PFAS) as a contaminant of emerging concern in surface water: A transboundary review of their occurrences and toxicity effects, J. Hazard. Mater. 419 (2021), 126361.
[34] H.R. Li, A.L. Junker, J.Y. Wen, L. Ahrens, M. Sillanpaa, J.Y. Tian, F.Y. Cui, L. Vergeynst, Z.S. Wei, A recent overview of per- and polyfluoroalkyl substances (PFAS) removal by functional framework materials, Chem. Eng. J. 452 (2023), 139202.
[35] J. Gluge, M. Scheringer, I.T. Cousins, J.C. DeWitt, G. Goldenman, D. Herzke, R. Lohmann, C.A. Ng, X. Trier, Z.Y. Wang, An overview of the uses of per- and polyfluoroalkyl substances (PFAS), Environ. Sci.-Process Impacts 22 (2020) 2345–2373.
[36] K.E. Pelch, A. Reade, T.A.M. Wolffe, C.F. Kwiatkowski, PFAS health effects database: Protocol for a systematic evidence map, Environ. Int. 130 (2019), 104851.
[37] I.T. Cousins, J.C. DeWitt, J. Gluge, G. Goldenman, D. Herzke, R. Lohmann, M. Miller, C.A. Ng, M. Scheringer, L. Vierke, Z.Y. Wang, Strategies for grouping per- and polyfluoroalkyl substances (PFAS) to protect human and environmental health, Environ. Sci.-Process Impacts 22 (2020) 1444–1460.
[38] S. Verma, T. Lee, E. Sahle-Demessie, M. Ateia, M.N. Nadagouda, Recent advances on PFAS degradation via thermal and nonthermal methods, Chem. Eng. J. Adv. 13 (2023), 100421.
[39] R. Lohmann, I.T. Cousins, J.C. DeWitt, J. Gluge, G. Goldenman, D. Herzke, A. B. Lindstrom, M.F. Miller, C.A. Ng, S. Patton, M. Scheringer, X. Trier, Z.Y. Wang, Are fluoropolymers really of low concern for human and environmental health and separate from other PFAS? Environ. Sci. Technol. 54 (2020) 12820–12828.
[40] B. Bayarkhuu, J. Byun, Optimization of coagulation and sedimentation conditions by turbidity measurement for nano- and microplastic removal, Chemosphere 306 (2022), 135572.
[41] H.Y. Sun, R.Y. Jiao, D.S. Wang, The difference of aggregation mechanism between microplastics and nanoplastics: Role of Brownian motion and structural layer force, Environ. Pollut. 268 (2021), 115942.
[42] N. Singh, E. Tiwari, N. Khandelwal, G.K. Darbha, Understanding the stability of nanoplastics in aqueous environments: effect of ionic strength, temperature, dissolved organic matter, clay, and heavy metals, Environ.-Sci, Nano 6 (2019) 2968–2976.
[43] X. Li, E.K. He, K. Jiang, W. Peijnenburg, H. Qiu, The crucial role of a protein corona in determining the aggregation kinetics and colloidal stability of polystyrene nanoplastics, Water Res. 190 (2021), 116742.
[44] S.N. Zhang, X.C. Guo, S.Y. Lu, J. He, Q. Wu, X.H. Liu, Z.Y. Han, P. Xie, Perfluorohexanoic acid caused disruption of the hypothalamus-pituitary-thyroid axis in zebrafish larvae, Ecotox. Environ. Safe. 232 (2022) 8.
[45] A.B.D. Nandiyanto, A. Suhendi, T. Ogi, T. Iwaki, K. Okuyama, Synthesis of additive-free cationic polystyrene particles with controllable size for hollow template applications, Colloid Surf. A-Physicochem. Eng. Asp. 396 (2012) 96–105.
[46] D.S. Yun, H.S. Lee, H.G. Jang, J.W. Yoo, Controlling size and distribution for nano-sized polystyrene spheres, Bull. Korean Chem. Soc. 31 (2010) 1345–1348.
[47] A.V. Delgado, F. Gonzalez-Caballero, R.J. Hunter, L.K. Koopal, J. Lyklema, Measurement and interpretation of electrokinetic phenomena, J. Colloid Interface Sci. 309 (2007) 194–224.
[48] H. Holthoff, S.U. Egelhaaf, M. Borkovec, P. Schurtenberger, H. Sticher, Coagulation rate measurements of colloidal particles by simultaneous static and dynamic light scattering, Langmuir 12 (1996) 5541–5549.
[49] P.A. Hassan, S. Rana, G. Verma, Making sense of Brownian motion: Colloid characterization by dynamic light scattering, Langmuir 31 (2015) 3–12.
[50] A. Tiraferri, M. Borkovec, Probing effects of polymer adsorption in colloidal particle suspensions by light scattering as relevant for the aquatic environment: An overview, Sci. Total Environ. 535 (2015) 131–140.
[51] P. Rouster, M. Pavlovic, I. Szilagyi, Destabilization of titania nanosheet suspensions by inorganic salts: Hofmeister series and Schulze-Hardy rule, J. Phys. Chem. B 121 (2017) 6749–6758.
[52] G. Trefalt, I. Szilagyi, M. Borkovec, Poisson-Boltzmann description of interaction forces and aggregation rates involving charged colloidal particles in asymmetric electrolytes, J. Colloid Interface Sci. 406 (2013) 111–120.
[53] G. Varga, Z. Somosi, A. Kukovecz, Z. Konya, I. Palinko, I. Szilagyi, A colloid chemistry route for the preparation of hierarchically ordered mesoporous layered double hydroxides using surfactants as sacrificial templates, J. Colloid Interface Sci. 581 (2021) 928–938.
[54] E. Gagliano, M. Sgroi, P.P. Falciglia, F.G.A. Vagliasindi, P. Roccaro, Removal of poly- and perfluoroalkyl substances (PFAS) from water by adsorption: Role of PFAS chain length, effect of organic matter and challenges in adsorbent regeneration, Water Res. 171 (2020), 115381.
[55] W.L. Yu, E. Matijevic, M. Borkovec, Absolute heteroaggregation rate constants by multiangle static and dynamic light scattering, Langmuir 18 (2002) 7853–7860.
[56] F.J. Montes Ruiz-Cabello, M. Moazzami-Gudarzi, M. Elzbieciak-Wodka, P. Maroni, C. Labbez, M. Borkovec, G. Trefalt, Long-ranged and soft interactions between charged colloidal particles induced by multivalent coions, Soft. Matter. 11 (2015) 1562–1571.
[57] F.J. Montes Ruiz-Cabello, G. Trefalt, P. Maroni, M. Borkovec, Accurate predictions of forces in the presence of multivalent ions by Poisson-Boltzmann theory, Langmuir 30 (2014) 4551–4555.
[58] F.J.M. Ruiz-Cabello, T. Oncsik, M.A. Rodriguez-Valverde, P. Maroni, M. Cabrerizo-Vilchez, Specific ion effects and pH dependence on the interaction forces between polystyrene particles, Langmuir 32 (2016) 11918–11927.
[59] C.F. Baes, R.E. Mesmer, The hydrolysis of cations, Krieger Publishing, Malabar, 1976.
[60] P.C. D'Haese, G. Douglas, A. Verhulst, E. Neven, G.J. Behets, B.A. Vervaet, K. Finsterle, M. Lurling, B. Spears, Human health risk associated with the management of phosphorus in freshwaters using lanthanum and aluminium, Chemosphere 220 (2019) 286–299.
[61] G. Trefalt, S.H. Behrens, M. Borkovec, Charge regulation in the electrical double layer: Ion adsorption and surface interactions, Langmuir 32 (2016) 380–400.
[62] T.C. Cao, T. Sugimoto, I. Szilagyi, G. Trefalt, M. Borkovec, Heteroaggregation of oppositely charged particles in the presence of multivalent ions, Phys. Chem. Chem. Phys. 19 (2017) 15160–15171.
[63] T. Sugimoto, T.C. Cao, I. Szilagyi, M. Borkovec, G. Trefalt, Aggregation and charging of sulfate and amidine latex particles in the presence of oxyanions, J. Colloid Interface Sci. 524 (2018) 456–464.
[64] B. Derjaguin, L.D. Landau, Theory of the stability of strongly charged lyophobic sols and of the adhesion of strongly charged particles in solutions of electrolytes, Acta Phys. Chim. 14 (1941) 633–662.
[65] G. Trefalt, Derivation of the inverse Schulze-Hardy rule, Phys. Rev. E 93 (2016), 032612.
[66] W.Y. Yu, N. Du, Y.T. Gu, J.G. Yan, W.G. Hou, Specific ion effects on the colloidal stability of layered double hydroxide single-layer nanosheets, Langmuir 36 (2020) 6557–6568.
[67] T.C. Cao, M. Borkovec, G. Trefalt, Heteroaggregation and homoaggregation of latex particles in the presence of alkyl sulfate surfactants, Colloids Interf. 4 (2020) 52.
[68] D. Takács, T. Péter, Z. Vargáné Árok, B. Katana, S. Papović, S. Gadzuric, M. Vraneš, I. Szilágyi, Structure-stability relationship in aqueous colloids of latex particles and gemini surfactants, J. Phys. Chem. B 126 (2022) 9095–9104.
[69] D.W. Fuerstenau, M. Colic, Self-association and reverse hemimicelle formation at solid-water interfaces in dilute surfactant solutions, Colloid Surf. A 146 (1999) 33–47.
[70] M. Kobayashi, S. Yuki, Y. Adachi, Effect of anionic surfactants on the stability ratio and electrophoretic mobility of colloidal hematite particles, Colloid Surf. A 510 (2016) 190–197.